Micro-Scale Simulation of Microstructural Evolution in Aluminum 1050 Using Crystal Plasticity Analysis

M.J. Rezaei, M. Sedighi*

[1] School of Mechanical Engineering, Iran University of Science and Technology, Iran

* Corresponding author: Sedighi@iust.ac.ir

[DOI: 10.22068/ijmse.4070]

Abstract:

The investigation of the mechanical response and microstructural evolution of engineering materials at the micro-scale under macro-scale loading poses a significant challenge in mechanical engineering, particularly in the fields of material forming and materials science. This critical has been addressed using a computational crystal plasticity tool known as DAMASK (Düsseldorf Advanced Material Simulation Kit). DAMASK is a multi-scale computational framework developed for modeling the deformation of crystalline materials by employing the principles of continuum mechanics and crystal plasticity. This software is widely recognized within the scientific community for its high flexibility and capability to simulate complex material behavior under various loading conditions. In this study, the DAMASK code—a finite element crystal plasticity software—was employed to analyze a representative volume element (RVE) containing 1000 grains under tensile loading. By applying a random initial texture to aluminum grade 1050, the microstructural evolution of the material under the specified loading conditions was evaluated. The results indicate the formation of <111> and <100> fiber textures in the (111) crystallographic plane of the FCC-structured material, which are consistent with observations obtained from EBSD experiments.

Keywords:

Crystal plasticity finite element method, Texture evolution, Tensile loading.

[DOI: 10.22068/ijmse.4070]

1. Introduction

Crystal plasticity (CP) is a meso-scale computational technique (at the crystal scale) that accounts for crystallographic anisotropy (crystal orientation) when modeling the mechanical behavior of polycrystalline materials [1]. CP adopts a microscopic approach to describe the formation of plastic flow and is commonly employed to investigate deformation mechanisms, particularly slip. Crystal plasticity models establish the stress-strain relationship at the crystal level in engineering materials and can therefore be used to predict a material's stress-strain response, texture evolution, and micromechanical behavior [2–4]. The superiority of crystal plasticity models over conventional constitutive models arises from several key aspects. First, they explicitly consider crystallographic slip as the fundamental mechanism of plastic deformation. Second, they provide a physically consistent framework for modeling plasticity based on the mechanics of deformation. Finally, because they capture the behavior of metals at the crystal level, CP models yield more accurate and physically meaningful predictions compared with traditional macroscopic approaches [5].

Two widely used formulations exist in crystal plasticity theory. The first is the finite element formulation, commonly known as the Crystal Plasticity Finite Element Method (CPFEM), which is based on the small-strain formulation and is primarily applied to problems in the field of mechanics [6,7]. The second is the spectral formulation, known as Crystal Plasticity Fast Fourier Transform (CPFFT), which utilizes Fast Fourier Transform techniques [8,9].

One of the earliest studies in the field of CPFEM can be attributed to the work of Bate [10]. This research highlighted the capabilities of CPFEM in analyzing intragranular plastic deformation textures and the effect of dislocation density on low- and high-angle grain boundaries.

[DOI: 10.22068/ijmse.4070]

Subsequently, Pai et al. modeled the uniaxial tensile deformation of polycrystalline aluminum using CPFEM [11]. They implemented crystal plasticity theory at the meso-scale on the specimen under investigation by employing the commercial software ABAQUS and the UMAT subroutine. In another study, Liu et al. compared the CPFEM and CPFFT methods for predicting the texture evolution during plane-strain compression tests [12]. The work by Kanjarla et al. focused on utilizing various structural models to investigate the mechanical response and microstructural evolution [13]. They evaluated the heterogeneity of plastic deformation in crystal interaction models using CPFEM. Wang et al. predicted deformation textures using the Taylor model [14], while Zhang and Joshi conducted a detailed micromechanical analysis of pure magnesium single crystals using a phenomenological structural model [15]. Their study examined both dislocation slip and twinning mechanisms during deformation. Numerous studies have explored microstructural evolutions induced by plastic deformation under various loading conditions [16–20]. These studies demonstrated the strong capability of CPFEM in solving complex loading scenarios. Additionally, the use of DAMASK for crystal plasticity simulations has gained significant attention in recent years due to its high efficiency in capturing microstructural transformations. This has made it a popular tool among researchers in materials and mechanical engineering [21–24].

The present study aims to investigate the microstructural evolution of a 1050-series aluminum alloy under uniaxial tensile loading with an initially random texture using the CPFE technique implemented in the Düsseldorf Advanced Material Simulation Kit (DAMASK). To simulate and analyze the material's mechanical behavior at the microstructural level, a representative volume element (RVE) containing 1000 crystals was used. The crystal plasticity simulations capture the complex interactions between grains and predict how these interactions influence the macroscopic

[DOI: 10.22068/ijmse.4070]

mechanical response of polycrystalline materials under tensile loading. The dynamic behavior of plastic flow and the hardening of face-centered cubic (FCC) crystalline materials are modeled using a phenomenological approach. Crystallographic anisotropy after loading is represented through polar figures (PF) and inverse pole figures (IPF). The obtained results are validated and compared with experimental data from EBSD analyses reported by other researchers.

2. Material and methods

Due to its widespread use across various industries, particularly in the power distribution, aluminum is extensively employed because of its low density and excellent electrical conductivity. According to the Energy Dispersive X-ray Spectroscopy (EDX) analysis, the sample investigated in this study is pure aluminum, Grade 1050, with a purity level exceeding 99.5% aluminum and containing trace amounts of elements such as manganese, iron, and silicon. The detailed chemical composition obtained from the EDX analysis is presented in the Table 1.

Table 1. Percentage of 1050 grade aluminum alloy compounds

Percentage of chemical composition %						
Al	Si	Fe	Cu	Mn	Cr	other
99.50	0.10	0.38	0.05	0.01	0.01	0.03

To determine the mechanical properties of the 6-mm diameter aluminum wire according to ASTM-E8M, a SANTAM uniaxial tension testing machine was utilized. The initial gauge length of the specimen was set at 100 mm, and the test was conducted at a strain rate of 0.001 1⁄s. The stress-strain curve obtained from the experimental uniaxial tensile test, along with the calibrated crystal plasticity model curve used to determine the elastic, plastic, and hardening parameters, is presented in Figure 1.

[DOI: 10.22068/ijmse.4070]

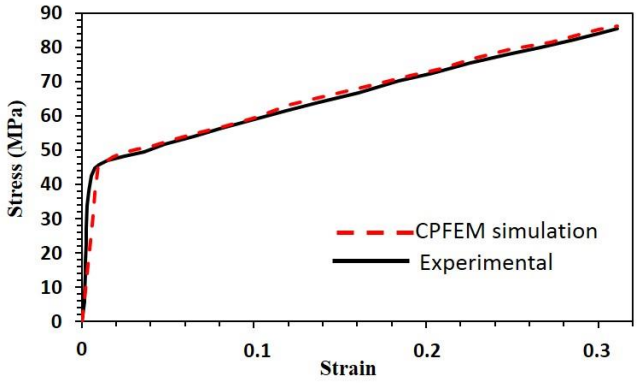

Figure 1. Comparison of stress-strain curves between experiment and CPFEM simulation for uniaxial tension

According to the graph in Figure 1, the yield stress of the sample is 45 MPa, and the tensile strength at a strain of 0.3 is 88 MPa. The maximum elongation of the sample is determined to be 0.35. The crystal plasticity structural model exhibits a high level of agreement with the elastic and plastic behavior observed in the experimental results.

A three-dimensional (3D) Voronoi method was employed to generate the representative volume element (RVE) containing 1,000 grains with random orientations, as shown in Figure 3(a). The 3D RVE was created using Neper software.

The stress-strain curve obtained from the crystal plasticity finite element simulation was compared with the experimental data, as illustrated in Figure 1. This comparison was used to calibrate the material parameters, including elastic, plastic, and hardening properties, for implementation in the DAMASK code. The calibrated material coefficients used in the DAMASK crystal plasticity simulations are listed in Table 2.

[DOI: 10.22068/ijmse.4070]

Table 2. The elastic, plastic, and hardening coefficients of the phenomenological constitutive model utilized in the DAMASK code

Parameters	Values
C_{11}	107.60 GPa
C_{12}	60.52 GPa
C_{44}	27.21 GPa
h_0	58 MPa
τ_s	63 MPa
$q^{\alpha\beta}$	1.40
τ_0	31 MPa
n	20
$\mathfrak{a}$	2.25

Crystallographic systems and the orientation of the crystal lattice are governed by micro-scale deformation mechanisms such as dislocation slip and twinning, which are fundamental phenomena investigated in crystal plasticity. During plastic deformation, it is generally assumed that dislocation slip occurs along the densest atomic planes, known as slip planes, and in the most closely packed atomic directions, referred to as slip directions. As illustrated in Figure 2, crystal plasticity theory (CP) describes plastic deformation as a process that produces permanent shape changes without altering the crystallographic orientation of the lattice. In contrast, elastic deformation is reversible, causing only temporary distortions in the lattice structure and corresponding changes in the crystallographic orientation.

[DOI: 10.22068/ijmse.4070]

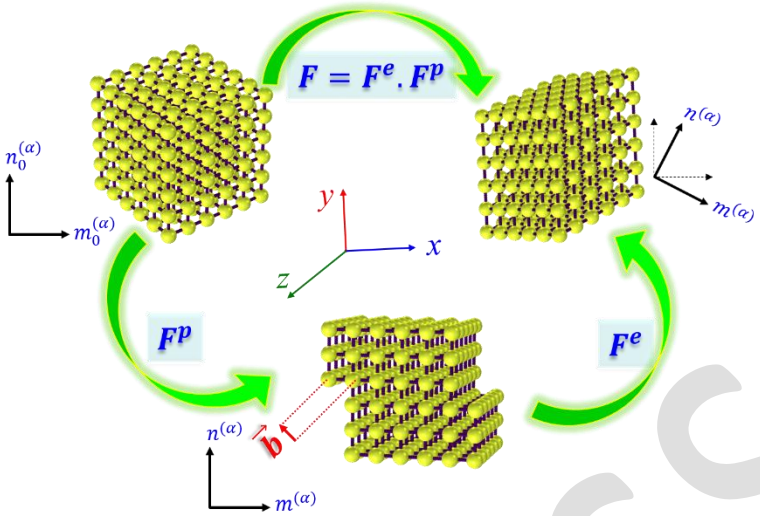

Figure 2. The hypothesis of crystal plasticity's deformation gradient, $F= F^e.F^p$

In crystal plasticity theory, the total deformation gradient is expressed as $\mathbf{F}= \mathbf{F}^e.\mathbf{F}^p$. Reversible lattice distortions are represented by the elastic deformation gradient ($\mathbf{F}^e$), whereas irreversible changes caused by dislocation slip and other mechanisms are described by the plastic deformation gradient ($\mathbf{F}^p$). A key concept in crystal plasticity is the multiplicative decomposition of the deformation gradient, which enables the separation of elastic and plastic effects. This formulation provides a robust foundation for modeling the complex deformation behavior of crystalline materials. In crystal plasticity, constitutive relationships often employ the material's elasticity tensor to relate the Second Piola–Kirchhoff stress tensor ($\mathbf{S}$) to the elastic Green strain tensor ($\mathbf{E}^e$). This framework allows the stress-strain relationship to incorporate anisotropy and directional properties inherent to the crystal structure. This formulation presented by Roters et al. [1], which has also been adopted in the present study, provides the theoretical basis for these relationships. Given the importance of governing mathematical equations in crystal plasticity, a summary of the relevant formulations is provided in this section. The Second Piola–Kirchhoff stress tensor can be obtained from the elastic Green strain tensor ($\mathbf{E}^e$) using the following relationship [1]:

[DOI: 10.22068/ijmse.4070]

$$\boldsymbol{S} = \mathbb{C}: \boldsymbol{E}^e \rightarrow \boldsymbol{E}^e = \frac{1}{2}(F^{eT}F^e - \mathrm{I}) \quad (1)$$

which $\mathbb{C}$ is the fourth-order anisotropic elastic stiffness tensor. The transposed gradient of elastic deformation is denoted byF^{eT}, and I is the identity matrix. The following represents the rate of change of $\mathbf{F}^{\mathrm{p}}$ [1]:

$$\dot{F}^p = L^p F^p \rightarrow L^p = \sum_{\alpha=1}^{N} \dot{\gamma}^\alpha m^\alpha \otimes n^\alpha \quad (2)$$

where L^p, α, N, and $\dot{\gamma}^\alpha$ denote the plastic deformation rate gradients, slip system, total number of slip systems, and shear rate on the α -th slip system, respectively. A key element in simulating slip deformation within specific crystallographic systems is the Schmid tensor, represented as $m^\alpha \otimes n^\alpha$. Here, m^α is the slip direction vector for the α-th slip system, n^α is the slip plane normal vector, and $\otimes$ denotes the dyadic product, which forms a second-order tensor from two vectors.

One of the most widely adopted constitutive models for predicting the dynamic behavior of plastic flow and the hardening of face-centered cubic (FCC) crystalline materials is the phenomenological power-law model, which is also employed in this study. A strain-rate-dependent power law is used to represent work hardening, relating the slip system strain rate to the ratio of resolved shear stress and critical resolved shear stress, as expressed below [16]:

$$\dot{\gamma}^a = \dot{\gamma}_0 \left|\frac{\tau^\alpha}{\tau_c^\alpha}\right|^{1/m} sgn(\tau^\alpha) \quad (3)$$

where $\dot{\gamma}_0$ is reference shear strain rate, and m is the slip rate sensitivity. The strain hardening on a specific slip system α is characterized by the evolution of the critical resolved shear stress τ_c^α, which is expressed by the following equation [16]:

$$\dot{\tau}_c^\alpha = \sum_{\beta=1}^{N} h^{\alpha\beta} \left|\dot{\gamma}^\beta\right| \quad (4)$$

where $\dot{\gamma}^\beta$ is the shear strain rate on the β -th slip system, and $h^{\alpha\beta}$ is the strain hardening matrix for the slip systems α and β, defined as follows [16]:

[DOI: 10.22068/ijmse.4070]

$$h^{\alpha\beta} = q^{\alpha\beta}\left[h_0\left(1-\frac{\tau_c^{\beta}}{\tau_s}\right)^{a}\right] \quad (5)$$

Here, h_0 is the initial hardening, τ_s is the saturated shear stress, a is the hardening parameter of the slip system, and $q^{\alpha\beta}$ is a 3×3 matrix ($\begin{bmatrix} A & \cdots & qA \\ \vdots & \ddots & \vdots \\ qA & \cdots & A \end{bmatrix}$) with 12 active slip systems during plastic deformation in FCC metals. This matrix defines the hardening interactions between different slip systems (α and β), where q represents the ratio of the self-hardening rate to the latent hardening rate.

Three-dimensional brick elements (C3D8) were used to mesh the representative volume element (RVE) containing 1000 crystals. A uniaxial tensile strain rate of 0.001 s^{-1} was applied to the aluminum RVE. The tensile loading simulation was performed in Abaqus, coupled with the DAMASK software for crystal plasticity finite element modeling (CPFEM), as illustrated in Figure 3(b).

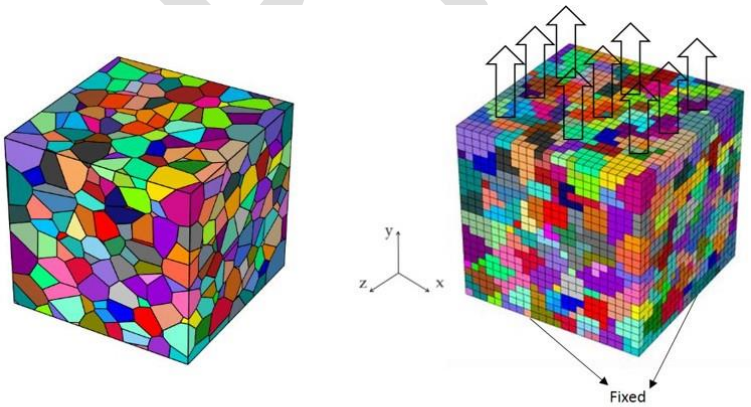

(a) (b)

Figure 3. a) A representative volume element containing 1000 crystals with a random distribution of crystal orientations, and b) Boundary conditions and loading on RVE

[DOI: 10.22068/ijmse.4070]

As shown in Figure 3(b), the lower face of the representative cube was fully constrained in six degrees of freedom, while the upper face was subjected to tensile loading, as illustrated in Figure 4.

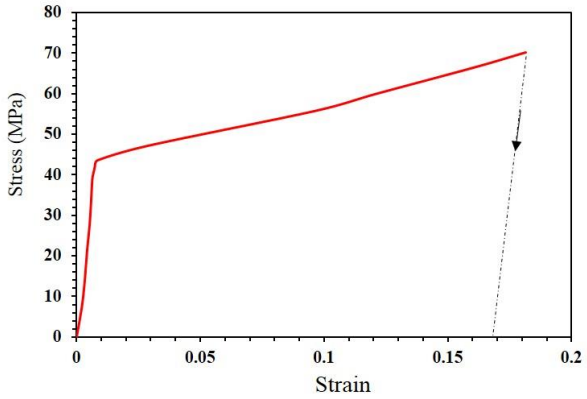

Figure 4. Loading and unloading condition on RVE containing 1000 crystals

The representative volume element (RVE) underwent a loading-unloading sequence to examine the texture evolution under tensile deformation, as shown in Figure 4. The loading–unloading curve presented in this figure was included to indicate the level of applied stress and the corresponding plastic strain during the tensile simulation. The unloading step was applied only to complete the stress–strain cycle and to illustrate the elastic recovery of the specimen.

3. Results and discussion

An initial random texture was assigned to the RVE containing 1000 crystals. This texture is illustrated as a pole figure for the (111) plane in Figure 5. Using the MTex toolbox available in MATLAB, the Euler angles were converted into a pole figure representation.

[DOI: 10.22068/ijmse.4070]

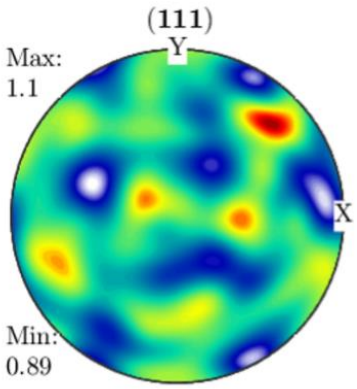

Figure 5. Random texture to RVE in initial increment of crystal plasticity finite element model

As shown in Figure 5, the absence of any distinct graphical pattern and the scattered crystal orientations of crystal orientation confirm the randomness of the initial texture. In other words, this indicates the sample possessed a completely random orientation distribution before loading.

The Euler angles of each crystal were extracted after solving the CPFEM model under the applied loading conditions shown in Figure 4. These angles are used to visualize the texture evolution through pole figures. By interpreting the resulting pole figure, the texture components developed within the sample can be identified. Since no additional plastic deformation occurs during unloading, the developed texture remains unchanged; therefore, the texture evolution analysis in this study focuses exclusively on the plastic deformation stage. The pole figure on the (111) crystallographic plane of the RVE after loading is presented in Figure 6. In this figure, the pole figure obtained from the CPFEM simulation is compared with the experimental pole figure derived from the EBSD test [11] to evaluate the model's accuracy.

[DOI: 10.22068/ijmse.4070]

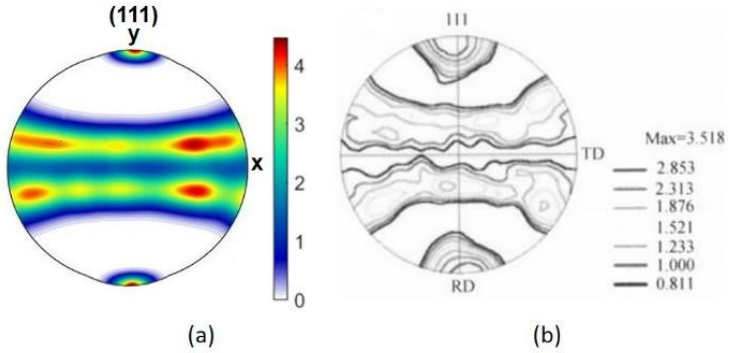

Figure 6. Pole figure in the crystallographic plane (111) under tensile loading a) CPFEM result and b) experimental result using EBSD [11]

The comparison between the results obtained from the CPFEM simulation and the experimental EBSD result is illustrated in Figure 6. By comparing the pole figures derived from the CPFEM solver and the experimental results with the ideal texture, it is observed that <111> and <100> fiber textures are formed on the (111) crystallographic plane of the aluminum sample subjected to tensile loading. The <111> fiber texture typically aligns with the direction of applied tensile load, indicating that the grains within the material have reoriented such that their <111> crystallographic direction preferentially aligns with the loading axis. The presence of <100> fiber texture suggests that some crystals are oriented with their <100> direction parallel to the loading axis or other sample directions. This texture commonly complements the <111> component, reflecting the diversity of grain reorientation mechanisms occurring during plastic deformation.

To further analyze the crystal orientation relative to the principal directions of the sample, inverse pole figures (IPFs) were used. The IPFs represent the preferred crystal orientation with respect to the rolling direction (RD), transverse direction (TD), and normal direction (ND) of the sample. Figure 7 illustrates the inverse pole figure (IPF) of the representative grain structure at a strain level of 0.17.

[DOI: 10.22068/ijmse.4070]

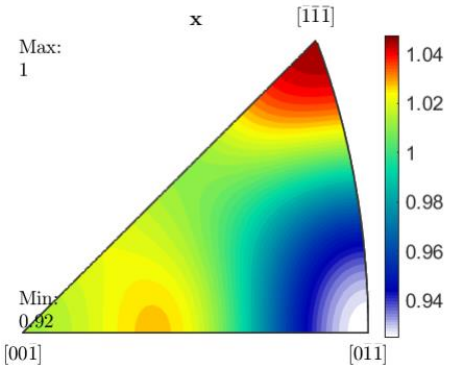

Figure 7. Inverse pole figure of [001], [011], and [111] crystal directions compared to the rolling direction of the sample (RD)

Figure 7 presents the inverse pole figure (IPF) along the rolling direction (RD) of the sample. It can be observed that most of the crystals in the representative volume element (RVE) are oriented along the [111] direction of the RD. Moreover, based on the orientation intensity near the [001] direction, it can be inferred that a fraction of the crystals are also oriented in this direction.

4. Conclusion

In this study, crystal plasticity finite element method (CPFEM) simulations were conducted to analyze the tensile loading response of a representative volume element (RVE) containing 1000 grains with a random initial texture. The results demonstrate that the crystal plasticity framework accurately predicts the microscopic responses of the material during tensile loading. Texture analysis revealed that, under loading, the grains of aluminum 1050 tend to align specific crystallographic orientations such as <111> and <100> within the (111) plane, which is consistent with the characteristic texture evolution of face-centered cubic (FCC) metals. Furthermore, the CPFEM analysis effectively captured the nonlinear mechanical behavior of the material, including the effects of slip-induced hardening and grain interactions. Overall, CPFEM simulations of the 1000-grains RVE with a random initial texture provide an efficient and reliable approach for

[DOI: 10.22068/ijmse.4070]

analyzing plastic deformation and predicting texture evolution under tensile loading. This methodology offers valuable insights for the design of advanced materials and optimization of mechanical performance across both micro- and macro scales. The finding confirm that the CPFEM model can accurately reproduce the nonlinear behavior of aluminum during tensile loading by accounting for slip mechanisms, grain interactions, and work hardening, thereby enhancing the understanding and prediction material behavior under various loading conditions.

[DOI: 10.22068/ijmse.4070]

References:

[1] F. Roters et al., "DAMASK–The Düsseldorf Advanced Material Simulation Kit for modeling multi-physics crystal plasticity, thermal, and damage phenomena from the single crystal up to the component scale," Comput. Mater. Sci., 2019, 158, 420–478, https://doi.org/10.1016/j.commatsci.2018.04.030.

[2] J. Li, X. Wu, and H. Jiang, "Crystal Plasticity Finite Element Simulation of Grain Evolution Behavior in Aluminum Alloy Rolling," Materials (Basel)., 2024, 17, 15, 3749, https://doi.org/10.3390/ma17153749.

[3] Y. Qu, Q. Zhao, and D. Ma, "Texture evolution and stress formation behaviour during tensile deformation using crystal plasticity finite element method," Mater. Sci. Technol., 2024, 26, 70-83, https://doi.org/10.1177/02670836241246663.

[4] Z. Tao et al., "Effects of specimen thickness and fiber length on tensile and cracking behavior of UHPFRC: Uniaxial tensile test and micromechanical modeling," Cem. Concr. Compos., 2025, 155, 105828, https://doi.org/10.1016/j.cemconcomp.2024.105828.

[5] N. Karar, "Usefulness of X-ray diffraction and Raman Spectra for understanding metal alloy microstructure repeatability," Indian J. Eng. Mater. Sci., 2024, http://nopr.niscpr.res.in/handle/123456789/64586.

[6] P. Areias, dos S. Charles, R. Melicio, and N. Silvestre, "An implicit staggered algorithm for CPFEM-based analysis of aluminum," J. Theor. Comput. Appl. Mech., 2024, https://doi.org/10.46298/jtcam.12960.

[7] S. Zhou, M. Ben Bettaieb, and F. Abed-Meraim, "A physically-based mixed hardening model for the prediction of the ductility limits of thin metal sheets using a CPFE approach," Int. J. Plast., 2024, 176, 103946, https://doi.org/10.1016/j.ijplas.2024.103946.

[8] A. Yamanaka, "Prediction of 3D microstructure and plastic deformation behavior in dual-phase steel using multi-phase field and crystal plasticity FFT methods," Key Eng. Mater., 2015, 651, 570–574, https://doi.org/10.4028/www.scientific.net/KEM.651-653.570.

[9] M. Kumar, A. Singh, and S. Mishra, "Enriching mean-field self-consistent texture simulations using the full-field FFT model," Mater. Sci. Technol., 2021, 37, 17, 1343–1352, https://doi.org/10.1080/02670836.2021.2007455.

[10] P. Bate, "Modelling deformation microstructure with the crystal plasticity finite–element method," Philos. Trans. R. Soc. London. Ser. A Math. Phys. Eng. Sci., 1999, 357, 1756, 1589–1601, https://doi.org/10.1098/rsta.1999.0391.

[11] H. Pi, J. Han, C. Zhang, A. K. Tieu, and Z. Jiang, "Modeling uniaxial tensile deformation of polycrystalline Al using CPFEM," J. Univ. Sci. Technol. Beijing, Miner. Metall. Mater., 2008, 15, 1, 43–47, https://doi.org/10.1016/S1005-8850(08)60009-2.

[12] B. Liu, D. Raabe, F. Roters, P. Eisenlohr, and R. A. Lebensohn, "Comparison of finite element and fast Fourier transform crystal plasticity solvers for texture prediction," Model. Simul. Mater. Sci. Eng., 2010, 18, 8, 85005, https://doi.org/10.1088/0965-0393/18/8/085005.

[13] A. K. Kanjarla, P. Van Houtte, and L. Delannay, "Assessment of plastic heterogeneity in grain

[DOI: 10.22068/ijmse.4070]

interaction models using crystal plasticity finite element method," Int. J. Plast., 2010, 26, 8, 1220–1233, https://doi.org/10.1016/j.ijplas.2009.05.005.

[14] P. Van Houtte, S. Li, M. Seefeldt, and L. Delannay, "Deformation texture prediction: from the Taylor model to the advanced Lamel model," Int. J. Plast., 2005, 21, 3, 589–624, https://doi.org/10.1016/j.ijplas.2004.04.011.

[15] J. Zhang and S. P. Joshi, "Phenomenological crystal plasticity modeling and detailed micromechanical investigations of pure magnesium," J. Mech. Phys. Solids, 2012, 60, 5, 945–972, https://doi.org/10.1016/j.jmps.2012.01.005.

[16] M. J. Rezaei, M. Sedighi, and M. Pourbashiri, "Developing a new method to represent the low and high angle grain boundaries by using multi-scale modeling of crystal plasticity," J. Alloys Compd., 2023, 939, 168844, https://doi.org/10.1016/j.jallcom.2023.168844.

[17] S. Mishra, F. Khan, and S. K. Panigrahi, "A crystal plasticity based approach to establish role of grain size and crystallographic texture in the Tension–Compression yield asymmetry and strain hardening behavior of a Magnesium–Silver–Rare Earth alloy," J. Magnes. Alloy., 2022, 10, 9, 2546–2562, https://doi.org/10.1016/j.jma.2021.08.021.

[18] N. C. Ferreri et al., "In-situ high-energy X-ray diffraction and crystal plasticity modeling to predict the evolution of texture, twinning, lattice strains and strength during loading and reloading of beryllium," Int. J. Plast., 2022, 150, 103217, https://doi.org/10.1016/j.ijplas.2022.103217.

[19] D. Hu, Z. Guo, N. Grilli, A. Tay, Z. Lu, and W. Yan, "Understanding the strain localization in additively manufactured materials: Micro-scale tensile tests and crystal plasticity modeling," Int. J. Plast., 2024, 177, 103981, https://doi.org/10.1016/j.ijplas.2024.103981.

[20] G. Chen et al., "Crystal plasticity finite element method investigation of normal tensile deformation anisotropy in rolled pure titanium sheet," Thin-Walled Struct., 2024, 200, 111904, https://doi.org/10.1016/j.tws.2024.111904.

[21] A. I. Aria, B. Holmedal, T. Mánik, and K. Marthinsen, "A Full-Field Crystal Plasticity Study on the Bauschinger Effect Caused by Non-Shearable Particles and Voids in Aluminium Single Crystals," Metals (Basel)., 2024, 14, 4, 424, https://doi.org/10.3390/met14040424.

[22] F. Qayyum, A. A. Chaudhry, S. Guk, M. Schmidtchen, R. Kawalla, and U. Prahl, "Effect of 3D representative volume element (RVE) thickness on stress and strain partitioning in crystal plasticity simulations of multi-phase materials," Crystals, 2020, 10, 10, p. 944, https://doi.org/10.3390/cryst10100944.

[23] K. Sedighiani et al., "Large-deformation crystal plasticity simulation of microstructure and microtexture evolution through adaptive remeshing," Int. J. Plast., 2021, 146, 103078, https://doi.org/10.1016/j.ijplas.2021.103078.

[24] P. Shanthraj et al., "Spectral solvers for crystal plasticity and multi-physics simulations," Handb. Mech. Mater. Springer, Berlin, 2019, 978–981,

[DOI: 10.22068/ijmse.4070]